GLOBAL CHANGE BIOLOGY
BIOENERGY

GCB Bioenergy (2017) **9**, 1024–1041, doi: 10.1111/gcbb.12403

A realistic meteorological assessment of perennial biofuel crop deployment: a Southern Great Plains perspective

MELISSA WAGNER[1], MENG WANG[2], GONZALO MIGUEZ-MACHO[3], JESSE MILLER[4], ANDY VANLOOCKE[5], JUSTIN E. BAGLEY[6], CARL J. BERNACCHI[4,7] and MATEI GEORGESCU[1,2]

[1]*School of Geographical Sciences and Urban Planning, Arizona State University, Tempe, AZ 85287-5302, USA,* [2]*School of Mathematical and Statistical Sciences, Arizona State University, Tempe, AZ, USA,* [3]*Universidade de Santiago de Compostela, Galicia, Spain,* [4]*Department of Plant Biology, University of Illinois, Urbana, IL, USA,* [5]*Department of Agronomy, Iowa State University, Ames, IA, USA,* [6]*Climate and Ecosystems Science Division, Lawrence Berkeley National Laboratory, Berkeley, CA, USA,* [7]*Global Change and Photosynthesis Research Unit, United States Department of Agriculture Agricultural Research Service, Urbana, IL 61801, USA*

Abstract

Utility of perennial bioenergy crops (e.g., switchgrass and miscanthus) offers unique opportunities to transition toward a more sustainable energy pathway due to their reduced carbon footprint, averted competition with food crops, and ability to grow on abandoned and degraded farmlands. Studies that have examined biogeophysical impacts of these crops noted a positive feedback between near-surface cooling and enhanced evapotranspiration (ET), but also potential unintended consequences of soil moisture and groundwater depletion. To better understand hydrometeorological effects of perennial bioenergy crop expansion, this study conducted high-resolution (2-km grid spacing) simulations with a state-of-the-art atmospheric model (Weather Research and Forecasting system) dynamically coupled to a land surface model. We applied the modeling system over the Southern Plains of the United States during a normal precipitation year (2007) and a drought year (2011). By focusing the deployment of bioenergy cropping systems on marginal and abandoned farmland areas (to reduce the potential conflict with food systems), the research presented here is the first realistic examination of hydrometeorological impacts associated with perennial bioenergy crop expansion. Our results illustrate that the deployment of perennial bioenergy crops leads to widespread cooling (1–2 °C) that is largely driven by an enhanced reflection of shortwave radiation and, secondarily, due to an enhanced ET. Bioenergy crop deployment was shown to reduce the impacts of drought through simultaneous moistening and cooling of the near-surface environment. However, simulated impacts on near-surface cooling and ET were reduced during the drought relative to a normal precipitation year, revealing differential effects based on background environmental conditions. This study serves as a key step toward the assessment of hydroclimatic sustainability associated with perennial bioenergy crop expansion under diverse hydrometeorological conditions by highlighting the driving mechanisms and processes associated with this energy pathway.

Keywords: biofuel crops, drought, hydroclimate, land-use change, modeling, renewable energy

Received 1 June 2016 and accepted 26 July 2016

Introduction

The U.S. Energy Independence and Security Act of 2007 (RFA, 2010) mandates the production of 80 gigaliters of ethanol from nongrain sources by 2022 (Gelfand *et al.*, 2013; Oikawa *et al.*, 2015). Perennial bioenergy crops have the potential to contribute an important relative share of U.S. ethanol demand, thereby helping to meet established mandates, while simultaneously decreasing reliance on fossil fuels. Reduced carbon emissions, increased energy security, and stabilization in energy pricing serve as key elements driving continued interest in the generation of biomass-derived energy (Haberl *et al.*, 2010; López-Bellido *et al.*, 2014; Abraha *et al.*, 2015; Miller *et al.*, 2015; Hudiburg *et al.*, 2016). Nongrain perennial biofuel crops such as the perennial grasses switchgrass (*Panicum virgatum*) and miscanthus (e.g., *Miscanthus* × *giganteus*) are particularly appealing due to their reduced carbon footprint, averted competition

Correspondence: Matei Georgescu, tel. 480 727 5986, fax 480 965 8313, e-mail: Matei.Georgescu@asu.edu

with food crops, minimal fertilizer usage and upkeep, and ability to grow on abandoned and degraded farmlands (Foley *et al*., 2005; Davis *et al*., 2012; Campbell *et al*., 2013; Bagley *et al*., 2014; Hudiburg *et al*., 2015; Vanloocke *et al*., 2010). By reducing greenhouse gas emissions, the deployment of perennial bioenergy crops could play an important role in mitigating anthropogenic climate change (Anderson-Teixeira *et al*., 2012).

In addition to biogeochemical impacts (e.g., Melillo *et al*., 2009; Gopalakrishnan *et al*., 2012), large-scale cultivation of perennial bioenergy crops will result in land use and land cover change (LULCC) impacts in which biogeophysical implications must be considered. Conversion of existing landscapes to perennial cropping systems will produce surface energy balance changes, affecting atmospheric boundary-layer dynamics (Weaver & Avissar, 2001), with implications for regional hydroclimate modification (Vanloocke *et al*., 2010; Georgescu and Lobell 2010; Georgescu *et al*., 2011; Georgescu *et al*., 2013; Pielke, 2001, 2005; Le *et al*., 2011; Xu *et al*., 2013; Bagley *et al*., 2014; Goldstein *et al*., 2014; Devaraju *et al*., 2015). The few studies that examined biogeophysical consequences of perennial biofuel crops used regional climate (e.g., Georgescu *et al*., 2009, 2011; Anderson *et al*., 2013; Khanal *et al*., 2013), ecosystem (e.g., Vanloocke *et al*., 2010; Le *et al*., 2011), and watershed-scale (Wagle & Kakani, 2014) models as well as micrometeorological assessments (e.g., Hickman *et al*., 2010; Abraha *et al*., 2015; Miller *et al*., 2015). These studies highlight the importance of time-varying representation that characterizes the distinct biofuel cropping systems appropriately (Bright *et al*., 2012, 2016). For example, recent field-scale plantation measurements of perennial biofuel crops illustrate greater albedo values during the growing season when compared with those of annual crops (e.g., maize and soybean) (Miller *et al*., 2015). Higher albedo values can lead to a decrease in net surface radiation and have been shown to regionally cool temperatures in climate modeling studies that replaced annual with perennial biofuel crops (Georgescu *et al*., 2009, 2011; Vanloocke *et al*., 2010; Bagley *et al*., 2015; Miller *et al*., 2015). This regional cooling was associated with both changes in the net surface radiation as well as the increased evapotranspiration (ET) resulting from the relatively denser and deeper rooting systems of perennial, relative to annual bioenergy crops, drawing down soil moisture from deeper soil depths (Vanloocke *et al*., 2010; Georgescu *et al*., 2011; Anderson *et al*., 2013; Hallgren *et al*., 2013; Ferchaud *et al*., 2015).

Enhanced ET and soil moisture depletion at deeper rooting depths could have important hydroclimate implications. Researchers have concluded that reduced surface runoff (McIsaac *et al*., 2010; Vanloocke *et al*., 2010; Chen *et al*., 2015) and the subsequent reductions in streamflow (Anderson *et al*., 2013; Goldstein *et al*., 2014; Khanal *et al*., 2014; Feng *et al*., 2015) are direct consequences of the diminished soil water volume. This reduction, according to Ferchaud *et al.* (2015) and Feng *et al.* (2015), could be compensated by lower soil moisture depletion near the surface, as a result of the denser canopy cover reducing soil evaporation. These suggestions are in agreement with recent modeling work that focused on the Cornbelt region (Georgescu *et al*., 2011) and Central Plains (Anderson *et al*., 2013) demonstrating increasing depletion of deep soil water volume for the Midwestern United States after the deployment of perennial bioenergy cropping systems. The aforementioned findings illustrate the potential for unintended consequences on the coupled atmosphere–hydrologic system and suggest that perennial biofuel expansion could lead to water stress and consequently lower yields (Vanloocke *et al*., 2010; Le *et al*., 2011; Anderson *et al*., 2013; Xu *et al*., 2013; Goldstein *et al*., 2014). Therefore, hydrometeorological assessments (e.g., near-surface temperature, surface energy balance, and soil moisture effects) are necessary to assess biophysical implications associated with large-scale deployment of perennial biomass energy crops.

The access to deeper soil moisture and enhanced ET relative to existing vegetation may reduce the need for irrigation for perennial biofuel crops in many regions (Miller *et al*., 2015) and could make these crops more resilient to drought. Under these conditions, the enhanced ET decreases atmospheric demand for water (Seneviratne *et al*., 2010), whereas access to deeper soil moisture mitigates plant stress due to water availability (Wu *et al*., 2002). Field measurements under drought conditions have reported the highest vapor deficits, highest ET-to-precipitation ratios, and lowest water-use efficiencies for perennial relative to annual cropping systems (Abraha *et al*., 2015). However, micrometeorological assessments of perennial biofuel crops have observed only small changes in albedo, ET, and yields when contrasting drought years to nondrought years (Abraha *et al*., 2015; Miller *et al*., 2015; Yimam *et al*., 2015), illustrating the enhanced resiliency of perennial systems (Joo *et al*., 2016). In fact, perennial crops outperformed annual biofuel crops with significantly higher leaf area index (LAI) and minimal crop damage during adverse hydrometeorological conditions (Miller *et al*., 2015). Early growing season precipitation proved an important factor in the availability of soil moisture (Wagle & Kakani, 2014) and crop yield (Yimam *et al*., 2015). Perennial biofuel crops, under a no-irrigation scenario, could reduce stress on already overburdened water resources and mitigate the effects of drought, especially in areas that have historically dealt with drought, such as the Southern High Plains.

Given the concerns associated with the diminished water resources, marginal lands are receiving additional recognition as a key component of a sustainable approach to biofuel crop expansion (Campbell *et al.*, 2008; Cai *et al.*, 2010; Zumkehr & Campbell, 2013). Although important in terms of improving process-level understanding, the majority of the aforementioned work has not provided a realistic representation of perennial biofuel crop expansion because these studies have generally focused on the replacement of existing annual with perennial biofuel crops. Planting perennial biofuel crops on marginal lands (i.e., land that would not be useful for annual crops) is a more sustainable approach because it averts competition with food production (Campbell *et al.*, 2008; Bagley *et al.*, 2014). Using marginal lands for biofuel production could decrease or negate the potential negative impacts on water resources (Feng *et al.*, 2015). However, the net effect of this pathway remains uncertain (Gelfand *et al.*, 2013; Rahman *et al.*, 2014) and requires site-specific examination of physical changes associated with varying deployment pathways.

Here, we perform the first realistic examination of hydrometeorological impacts associated with perennial bioenergy crop expansion and focus on land that would not useful for annual crops. Using a suite of simulations with a coupled land surface–atmosphere model, applied at a high resolution, we focus on the quantification of meteorological effects during a normal hydrologic year (2007) and a drought year (2011) for the Southern Plains of the United States (Hoerling *et al.*, 2013; United States Drought Monitor, 2014; Tadesse *et al.*, 2015). The historically drought-prone nature of this region serves as an ideal test-bed to examine the region's drought resiliency under an alternate land-use scenario. This study quantifies hydrometeorological impacts for varying scenarios of perennial biofuel crop expansion under diverse hydrometeorological conditions and will fill a critical void associated with bioenergy-based land-use conversion. This work sheds light on the sustainability of perennial bioenergy crop deployment over marginal and abandoned farmland areas and therefore contributes to the emerging body of literature characterizing the potential contribution of perennial biomass energy crops to the portfolio of renewable energy options.

Materials and methods

Regional climate model design

We used the Weather Research and Forecasting (WRF) model version 3.6.1 coupled with the Noah land surface model (LSM) to examine the potential effects of perennial biofuel crop expansion under normal climate and drought conditions for the years 2007 and 2011, respectively. WRF is a nonhydrostatic mesoscale model, commonly utilized in climate research and operational forecasting (Skamarock *et al.*, 2005). The Noah LSM calculates time-varying soil temperature and moisture, horizontally and vertically through a multilayer soil column extending down to 2 m, and specifies surface energy partitioning of available radiant energy to drive atmospheric processes and characterize the meteorological response to vegetation forcing (Ek *et al.* 2003). The LSM used in this work has been used to address a spectrum of topics ranging from the assessment of hypothetical bioenergy expansion (e.g., Georgescu *et al.*, 2011) to improving predictive capabilities through the strategic use of remote sensing data (e.g., Cao *et al.*, 2015). We used a triple nested grid configuration with the outermost and innermost domains utilizing 32- and 2-km grid spacing, respectively (see Fig. 1a). Centered over the northeastern part of Oklahoma, the innermost domain defines the boundaries of our study area and is discretized by 149 and 113 grid points in the east–west and north–south directions, respectively (see Fig. 1b). The city of Tulsa, Oklahoma, is located in the center of the study area and is surrounded predominantly by grasslands (see Fig. 1b).

We acquired Final Operational Global Analysis (FNL) data from the National Centers for Environmental Prediction for the years 2007 and 2011. FNL data are reanalysis data derived from observational weather data, Global Forecast System (GFS) model runs, and other analyses. These data are available from the Research Data Archive (http://rda.ucar.edu), are provided at 1-degree by 1-degree resolution on a global domain, and were used to initialize and force the lateral boundaries for the outermost domain for all WRF simulations. All simulations were initialized on December 1st of the preceding year and a one-month spin-up was performed to allow the system to reach a state of equilibrium. This initial month, for all experiments, was discarded, and only the 12 months pertaining to each year was used for the subsequent analysis.

Data used for model evaluation

We conducted an ensemble of model simulations by varying a suite of select physics schemes (microphysics and radiation) aimed at selecting an optimal control experiment (see Table 1). The convective scheme was not varied in this study, because convection is explicitly resolved in the innermost domain. Model performance metrics for temperature and precipitation were evaluated for each year using Taylor diagrams. The utility of Taylor diagrams stems from their simultaneous capability to summarize statistical measures of centered root mean square error (RMSE), normalized standard deviation, and correlation coefficient (Taylor, 2001). Metrics were based on the comparison between model simulations and observed meteorological data, which were obtained from seven stations available from the Global Historical Climate Network (see Table 2). Mean daily temperatures and daily precipitation totals were averaged over the seven stations and compared to the corresponding modeled grid cells.

In addition to evaluation against the observed station values, annual spatial patterns of total precipitation and average temperature were calculated. Model simulations were first

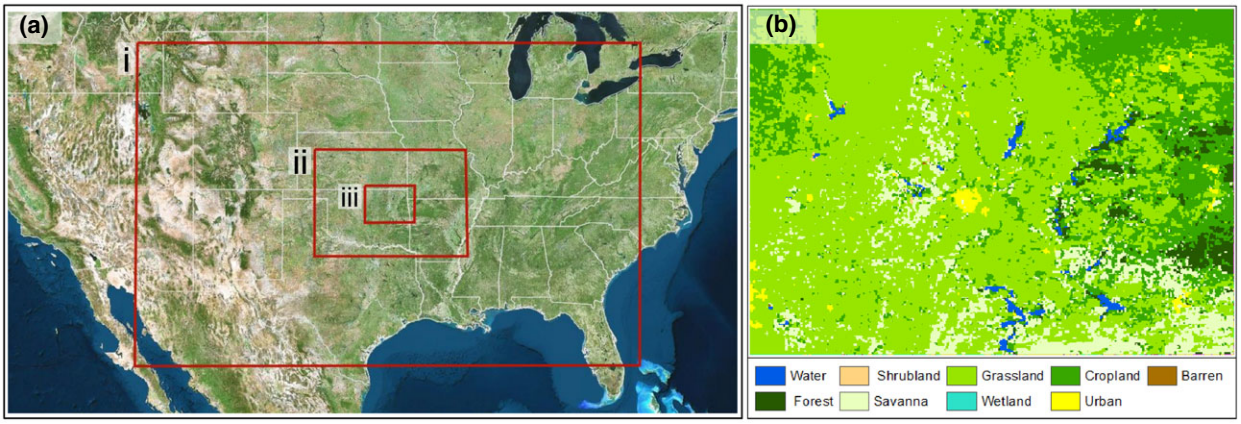

Fig. 1 (a) Study area showing triple nested configuration with (i) outermost (32-km grid spacing), (ii) middle (8-km grid spacing), and (iii) innermost (2-km grid spacing) domain resolution, respectively. (b) Innermost domain land use/land cover.

Table 1 List of model simulations and the configuration (microphysics, shortwave and longwave radiation schemes used to select an optimal control simulation)

Simulation	Microphysics	Shortwave radiation	Longwave radiation
1	WSM 3	Dudhia	RRTM
2	Thompson *et al.*	Dudhia	RRTM
3	Morrison 2-moment	Dudhia	RRTM
4	WDM 6-class	Dudhia	RRTM
5	Thompson *et al.*	RRTMG	RRTM
6	WDM 6-class	RRTMG	RRTM
7	Thompson *et al.*	RRTMG	RRTMG
8	WDM 6-class	RRTMG	RRTMG

Table 2 List of Global Historical Climatological Network stations by name and their location (latitude and longitude)

Station name	Latitude	Longitude
Mannford	36.17472	−96.44333
Spavinaw	36.38944	−95.05972
Bartlesville	36.76833	−96.02611
Pawhuska	36.66917	−96.34722
Tulsa Intl Airport	36.19944	−95.88722
Muskogee	35.65667	−95.36139
Ponca	36.73056	−97.09972

resampled from 2- to 4-km resolution to match the observed spatial gridded datasets obtained from the University of Idaho at 4-km grid spacing (Abatzoglou, 2013). For the simulated annual total precipitation, yearly model-aggregated values were divided by the observed yearly total precipitation to produce an annual precipitation ratio. We also calculated the average annual temperatures for the observed and simulated experiments to spatially assess the model performance. Simulated annual average temperature was subtracted from the observed annual average temperature, yielding average annual temperature differences.

Perennial biofuel crop suitability

To determine the locations for perennial biofuel deployment, we utilized bioenergy crop suitability data at 1-km resolution based on Cai *et al.* (2010). These data identify the marginal and abandoned lands suitable for biofuel crop deployment globally based on soil productivity, slope, soil temperature, humidity index, and land-use information. We chose the most realistic scenario, which included low-productivity grasslands, savanna, and shrublands with regular or marginal productivity, while excluding the total current pasture land and regions of crop production (see Fig. 2a). Extracting only information within the innermost domain, these data were resampled to 2-km resolution to match the gridded specification of our innermost domain. To ensure deployment over only marginal or abandoned farmlands, suitable locations were compared with the WRF land cover data [MODIS Modified International Geosphere-Biosphere Program (IGBP)] using a GIS platform. Any pixel coincident with agriculture was deemed unsuitable for deployment. Lastly, the suitability data were reclassified using quantile classification method into four suitability classes ranging from low to very high suitability.

We assume two deployment scenarios to examine the range of potential hydrometeorological impacts and associated uncertainty given a range of perennial bioenergy crop distribution. The first scenario employs the full perennial biofuel deployment as previously discussed and covers 56 667.2 square kilometers (see Fig. 2b). The second scenario limits the potential perennial biofuel deployment to the upper 25% of suitable areas, covering only 14 376.3 square kilometers (see Fig. 2c).

Biophysical representation of bioenergy crops and simulations performed

Perennial biofuel crop deployment was represented via the modification of biophysical parameters characteristic of perennial grasses: albedo, LAI, and vegetation fraction, or the fraction of vegetative cover within a 2-km grid cell, under a no-irrigation scenario. Using the observed field-scale values obtained from Miller *et al.* (2015), daily albedo data were

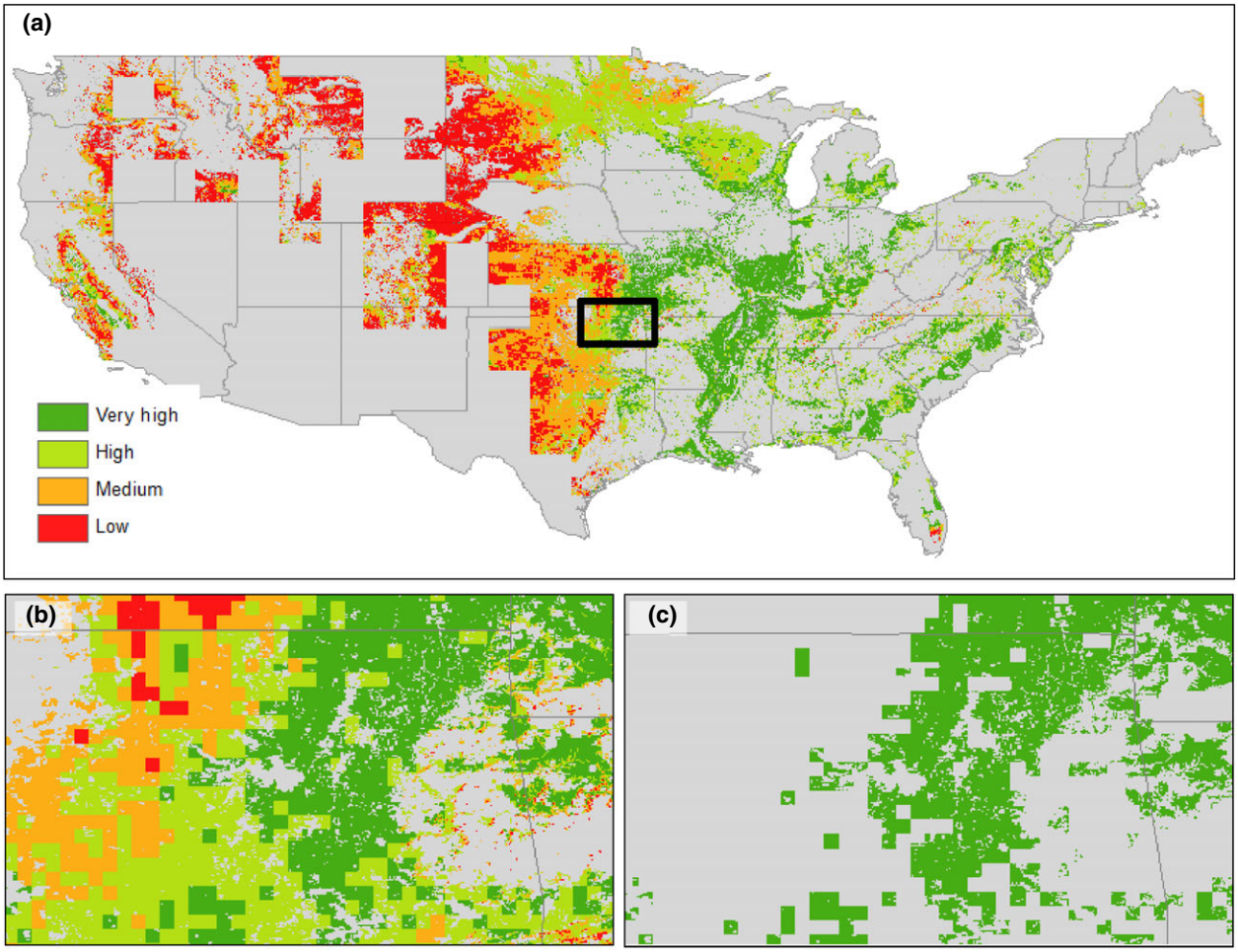

Fig. 2 Biofuel crop suitability for (a) contiguous United States using a quantile classification. Unsuitable locations are displayed in gray, while low and very high suitability locations are displayed in red and green, respectively. Potential perennial biofuel deployment for (b) 100% deployment scenario [all suitable classes presented in panel (a)] and (c) 25% deployment scenario (only very high suitability shown in green). The black box shown in (a) is the domain illustrated in (b) and (c).

averaged across the available sites for two plant types: switchgrass and miscanthus. A linear interpolation was applied to fill gaps separately for each year (2010 and 2011). These values were then averaged across plant types and over the two years, yielding mean daily albedo values for perennial biofuel crops (Fig. 3a). Mean daily albedo values were interpolated to three-hourly values (corresponding to the temporal frequency of WRF output) and ingested into WRF for both simulated years (2007 and 2011). When compared with albedo values of the existing land cover utilized for the control experiments (Fig. 3a), mean daily albedo values of perennial biofuel crops are higher. This difference is especially evident during the growing season from May to October.

LAI and vegetation fraction values were also modified to further characterize the realistic phenological evolution of perennial bioenergy cropping systems. These values were scaled to follow the changes in observed albedo values using the known maximum and minimum values (see Fig. 3b, c). From May to October, LAI values for perennial biofuel crops are 58% higher than LAI values of existing land cover. Unlike LAI, the differences in vegetation fraction between perennial biofuel crops and existing land cover are smaller, with vegetation fraction values approximately 20% higher than existing grasslands from May to October.

After the modification of albedo, LAI, and vegetation fraction, two sets of simulations were performed to examine the effect of perennial bioenergy crop deployment (see Table 3). The first set of simulations aimed to establish a baseline using existing land cover from the best (hereafter *Exp1*) and least (hereafter *Exp2*) skilled model configurations as compared to suitable station and gridded observational data (see Data used for model evaluation). This set was determined from an ensemble of eight simulations with varying physics options that regional climate models such as WRF are well known to be highly sensitive to (Table 1). The second set of simulations represented 100% and 25% perennial biofuel crop deployment scenarios in the respective suitable areas by modifying biophysical parameters of albedo, LAI, and vegetation fraction values. Additionally, each of the perennial bioenergy cropping system simulations (i.e., 100% and 25%) was conducted for Exp1 (i.e., most skilled

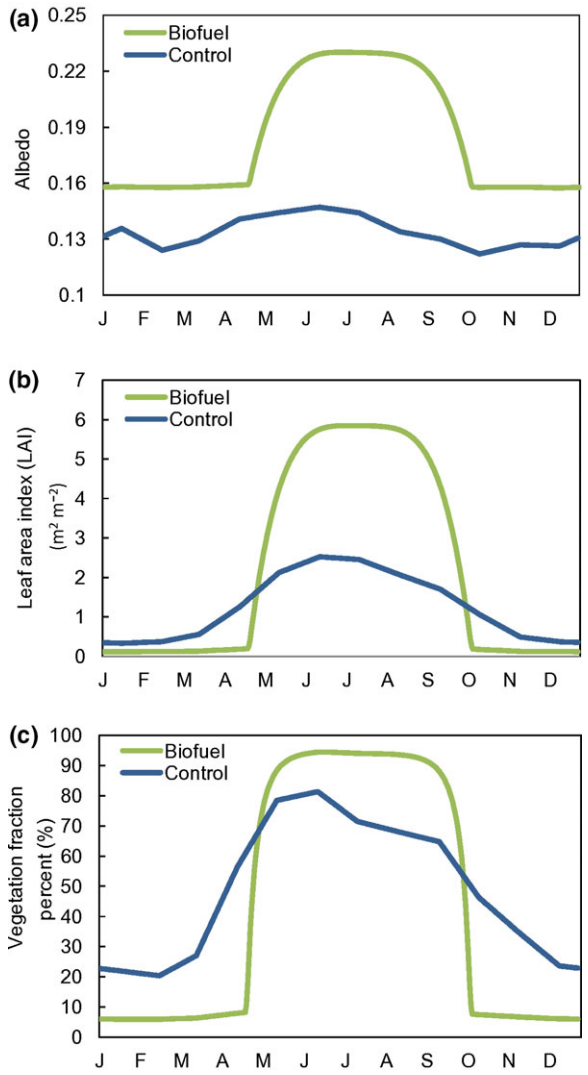

Fig. 3 Phenological evolution of biophysical parameters for existing grasslands and perennial biofuel representation: (a) albedo, (b) leaf area index (LAI), and (c) vegetation fraction. Default biophysical parameter representation (control) and perennial biofuel crop values are shown in solid blue and green lines, respectively.

control simulation: *Exp1_100* and *Exp1_25*) and Exp2 (i.e., least skilled control simulation: *Exp2_100* and *Exp2_25*). A full description of simulations performed with and without perennial biofuel crop deployment is presented in Table 3.

Table 3 List of model simulations with and without perennial biofuel crop deployment

WRF simulations	Scenario	Spin-up	Analysis time
Control	Simulation 6 (Exp1): best skill	Dec 1–31, 2006	Jan 1–Dec 31, 2007
	Simulation 1 (Exp2): least skill	Dec 1–31, 2010	Jan 1–Dec 31, 2011
Biofuel Deployment (Albedo, Veg Frac, LAI)	100%	Dec 1–31, 2006	Jan 1–Dec 31, 2007
	Simulation 6 (Exp1_100)	Dec 1–31, 2010	Jan 1–Dec 31, 2011
	Simulation 1 (Exp2_100)		
	25%		
	Simulation 6 (Exp1_25)		
	Simulation 1 (Exp2_25)		

Results

Model evaluation

Overall, WRF simulations demonstrated greater skill with temperature than with precipitation. The suite of ensemble members exhibited high skill in simulating near-surface temperatures as indicated by the high correlations – generally between 0.97 and 0.99 – and centered RMSE near 1 degree Celsius (see Fig. 4a, b). Modeled near-surface temperature performance was similarly skilled for both years, and the sensitivity to differing physical parameterizations was minimal. Unlike temperature, the sensitivity to the suite of examined physics parameterizations resulted in large variability in precipitation skill (Fig. 4c, d). During 2007 (see Fig. 4c), the correlation values varied between 0.30 and 0.40, indicating moderate skill. Simulation 4, employing WDM6 microphysics (i.e., single moment representation with six hydrometeor species), produced the highest correlation (0.40), lowest centered RMSE (0.97) and standard deviation (0.98), relative to the observed values. During 2011, the range of ensemble member performance indicated improved skill, with higher correlation values generally ranging between 0.55 and 0.65 (see Fig. 4d). Simulation 4, utilizing the WDM6 microphysics parameterization, exhibited one of the highest correlations and best matched the observed variance (dotted circle lines) and bias (solid blue lines), with values just shy of 1 demonstrating excellent simulation of day-to-day precipitation variability. Based on the aforementioned metrics, all ensemble members performed with high fidelity in their simulation of near-surface temperatures, while Simulation 4, making use of WDM6 microphysics, best demonstrated precipitation magnitude for both hydrometeorological years.

Examination of spatial characteristics of simulated meteorological variables can provide further confidence in simulation skill by illustrating geographically explicit performance. Spatial patterns of annually averaged temperature (Fig. 5) confirmed the previously demonstrated strong model skill for near-surface temperature. Small

differences were apparent between the observed mean annual temperatures for 2007 and 2011 and the suite of ensemble member simulations produced biases generally <2 °C. The differences among individual members were mainly attributable to the selection of shortwave radiation schemes. In 2007, Simulations 5–8 (Table 1 and Fig. 5e–h), utilizing RRTMG shortwave radiation scheme, produced a warm bias of 1.5–2.5 °C, whereas in 2011, Simulations 1–4 (Fig. 5i–l), utilizing Dudhia shortwave radiation scheme, produced a cold bias of 1.5–2.5 °C. Overall, the temperature differences attributable to microphysics schemes were more localized and generally <0.5 °C.

The selection of microphysics scheme was key to model performance of precipitation despite its apparent underestimation (Fig. 6). Simulation 1 with WSM-3 microphysics (see Table 1) produced the least model skill for both years with ratio values of 0.7 or less for most of the domain (Fig. 6a, i). For 2007, Simulation 3 with Morrison microphysics (Table 1) considerably overestimated the amount of precipitation in the eastern portion of the domain (Fig. 6c). Simulation 6 with WDM6 microphysics (see Table 1) also overestimated precipitation in the southeast corner during 2007 (see Fig. 6f), but the simulated overestimation was considerably less in magnitude and extent. For 2011, Simulation 6 with WDM6 microphysics (see Table 1) best captured the spatial extent and magnitude of observed rainfall (see Fig. 6h). Of the eight different model configurations, Simulation 6 demonstrated the greatest skill in modeling precipitation for both years, while Simulation 1 produced the least skill.

Although Simulation 4 had the best model skill in simulating precipitation according to station average metrics (Taylor diagrams), Simulation 6 best captured the spatial pattern of annual precipitation, and statistical metric differences between the pair of ensemble members were small. Both Simulation 4 and Simulation 6 used the WDM-6 microphysics scheme, but had different shortwave radiation schemes. Despite a slight warm bias in 2007, RRTMG shortwave radiation scheme used in Simulation 6 improved the overall spatial pattern of precipitation with minimal differences between the simulated and observed values.

Based on the aforementioned results, Simulation 6 was selected as the best representative control experiment (Exp1), whereas Simulation 1 was selected as the least performing member (Exp2). From this point forward, we utilize both Simulation 6 (Exp1) and Simulation 1 (Exp2) with different perennial biofuel crop deployment scenarios (see Table 3) to examine the sensitivity of bioenergy crop deployment.

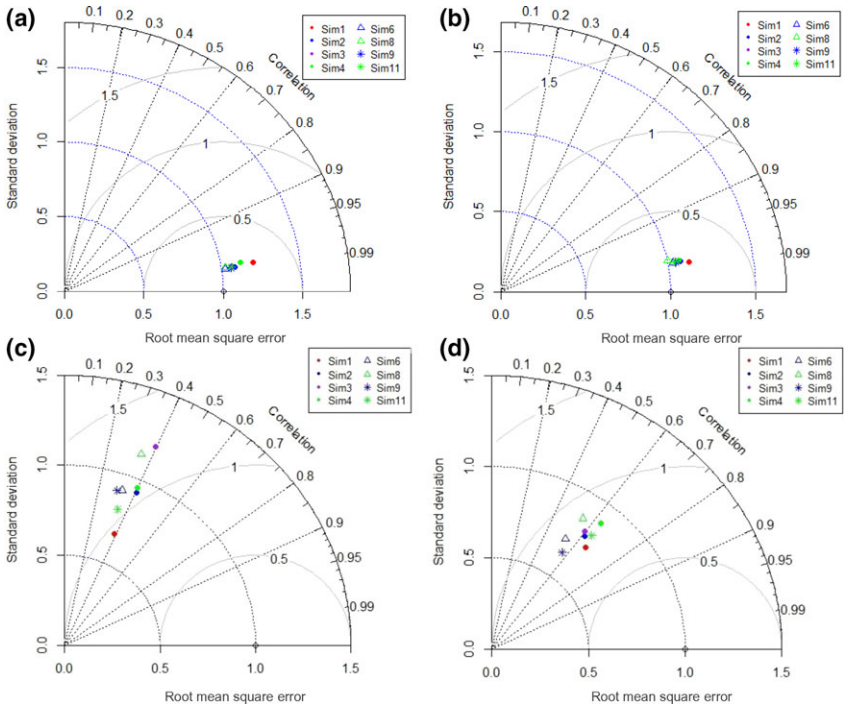

Fig. 4 Taylor diagrams of annual daily mean temperature between averaged observations and model grid points for (a) 2007 and (b) 2011 and annual daily precipitation for (c) 2007 and (d) 2011, where each symbol corresponds to model performance of the individual members presented in Table 1. Angular axis shows the spatial correlations between modeled and observed variables. Radial *x*-axis and *y*-axis show the normalized standard deviation and centered root mean square error (RMSE), respectively.

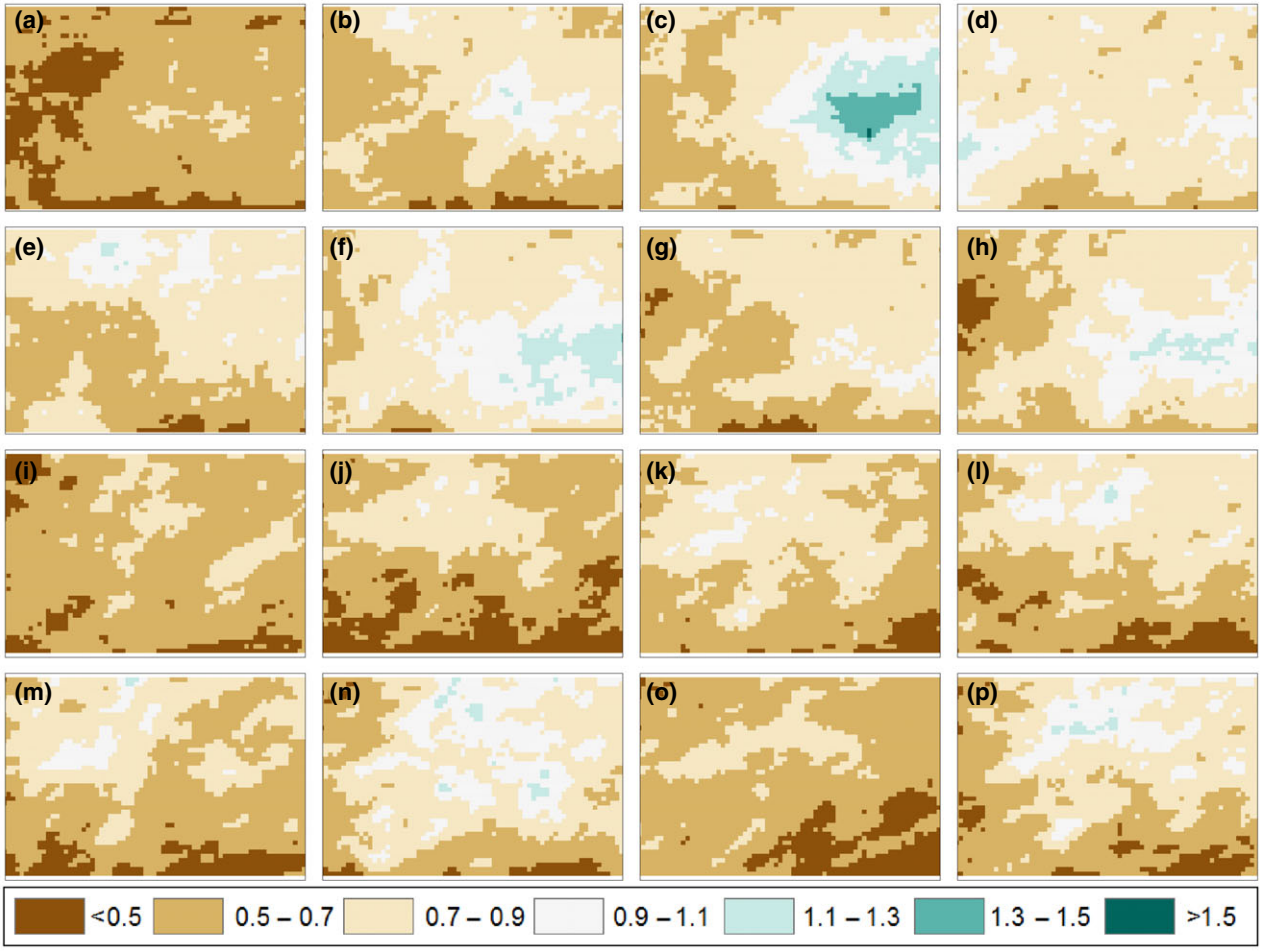

Fig. 5 Mean annual differences between the observed and modeled temperatures (°C). Figure (a–h) corresponds to the year 2007 and represents the Simulations 1–8 parameters (from left to right) as listed in Table 1. Figure (i–p) corresponds to the year 2011 and represents the Simulations 1–8 parameters (from left to right) as listed in Table 1.

Simulated impacts on temperature, ET, and soil moisture

The simulated impact of perennial bioenergy crop deployment indicates a decrease in near-surface air temperature for both normal hydrometeorological (2007) and drought (2011) years. For both years, time-series analyses of domain-averaged near-surface temperatures (i.e., 2 m temperatures; Fig. 7) show that the greatest temperature differences occurred during the growing season – from May to October – with a slight increase in temperatures from April to May, and October to November, when LAI values are lower for perennial bioenergy crops (see Fig. 3). Temperature decreases associated with perennial biofuel crop deployment were slightly more pronounced in 2007 (normal year) than in 2011 (drought year) with an average decrease of 1.0 °C compared with 0.80 °C, respectively. In 2007, the reduction in near-surface temperature associated with perennial bioenergy crop deployment frequently exceeded 1–1.5 °C during the growing season for both deployment scenarios. In terms of scenario and experimental differences, the reduction in near-surface temperature was greater for the full deployment scenario (i.e., Exp1_100 and Exp2_100) than for the partial deployment scenario (i.e., Exp1_25 and Exp2_25), while only minimal differences were apparent between Exp1 and Exp2 (i.e., the thermal impact of bioenergy crop deployment does not appear to be a function of model performance).

Because the largest simulated effects on near-surface temperature were apparent during the growing season, we examined the spatial impacts of temperature associated with perennial bioenergy crop deployment from May to October. For both simulated years, maximum temperature differences were more pronounced for the full deployment relative to the partial deployment scenario, consistent with the fraction of crop deployment (Fig. 8). Results for full deployment scenarios revealed a

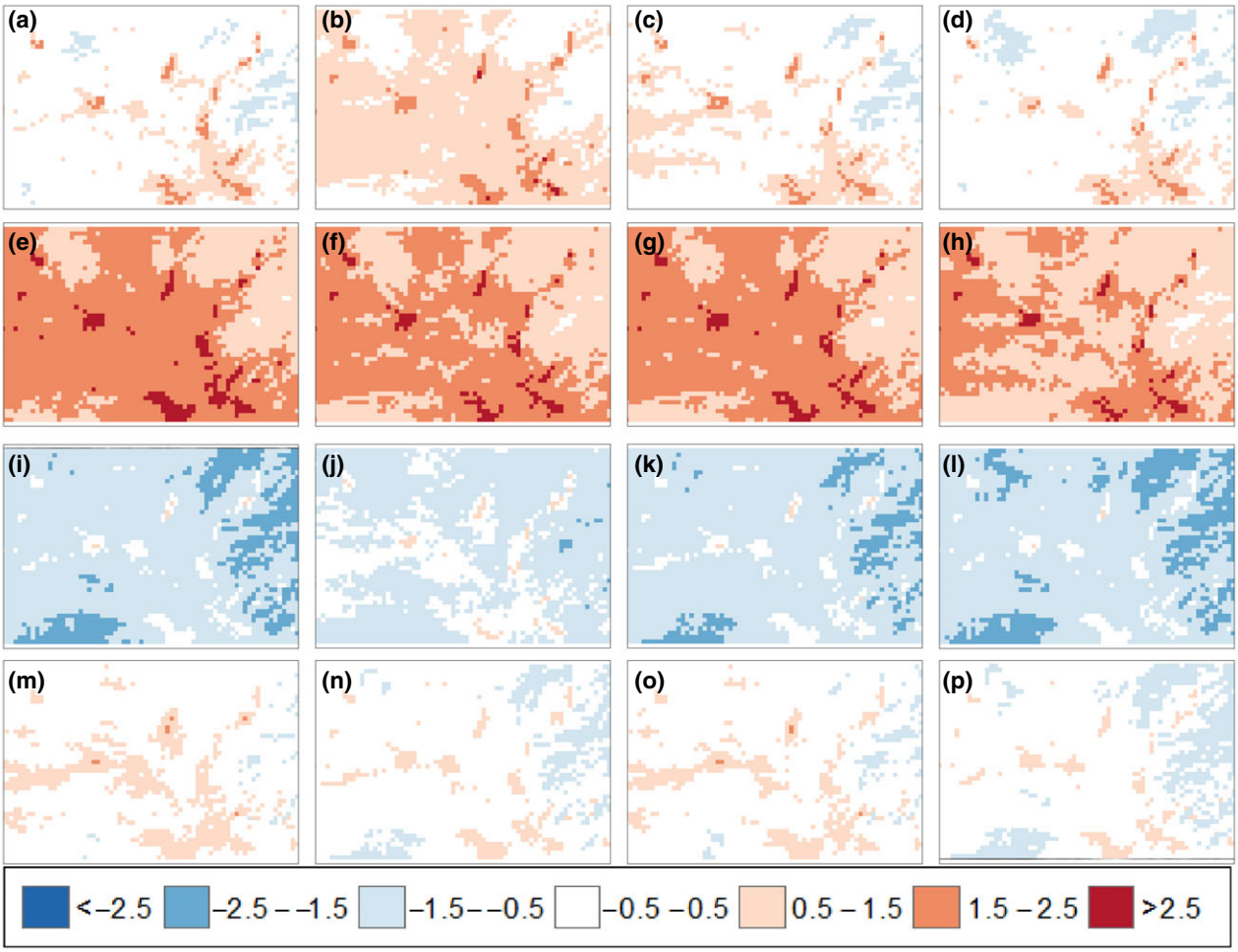

Fig. 6 Annual precipitation ratio (the total simulated precipitation divided by the total observed precipitation). Panel representation is same as in Fig. 5. Figures (a–h) correspond to the year 2007, and represent simulations 1–8 parameters (from left to right) as listed in Table 1. Figures (i–p) correspond to the year 2011, and represent simulations 1–8 parameters (from left to right) as listed in Table 1.

temperature decrease following a west–east gradient. In 2007, temperatures decreased by up to 1.8 and 0.7 °C in the west and east, respectively (Fig. 8e, f). In 2011, this gradient was slightly moderated with a corresponding 1.3 and 0.5 °C near-surface temperature decrease in the west and east, respectively (Fig. 8g, h). Temperature differences were more localized under the partial deployment compared with the full deployment scenario, despite the temperature decreases beyond deployment areas. Subtle differences were also observed between experiments, more notably with Exp1_25 and Exp2_25 in 2007 (Fig. 8a, b). Temperature decreases were slightly greater in the deployment areas for Exp1 compared with Exp2 with up to 1.3 °C of cooling compared with 1.1 °C, respectively. Moreover, Exp1 exhibited a stronger cooling signal extending well beyond the deployment area by up to 0.5 °C. Although the magnitude of cooling exhibited by Exp1 was noticeably greater than that of Exp2, the simulated spatial consistency between Exp1 and Exp2 indicates a limited sensitivity of bioenergy crop deployment to model performance.

Unlike temperature, simulated impacts of perennial bioenergy crop deployment show diverging results for ET based on model performance and climate year. Time-series analyses of domain-averaged ET (Fig. 9) indicate that simulation results (i.e., Exp1 and Exp2) diverge from the late spring to September 2007 (Fig. 9a). During this period, ET associated with Exp1_25 and Exp1_100 increased by an average of 0.73 mm day^{-1}, while ET associated with Exp2_25 and Exp2_100 decreased by an average of 0.19 mm day^{-1} (i.e., increased ET for Exp1 simulations, but decreased ET for Exp2 simulations). Simulated impacts of precipitation showed similarly diverging results, pointing to a positive signal with Exp1 and negative signal with Exp2 (see Fig. S1 and Table S1). However, because the standard deviation explained a greater fraction of the mean, there is reduced confidence in the robustness of

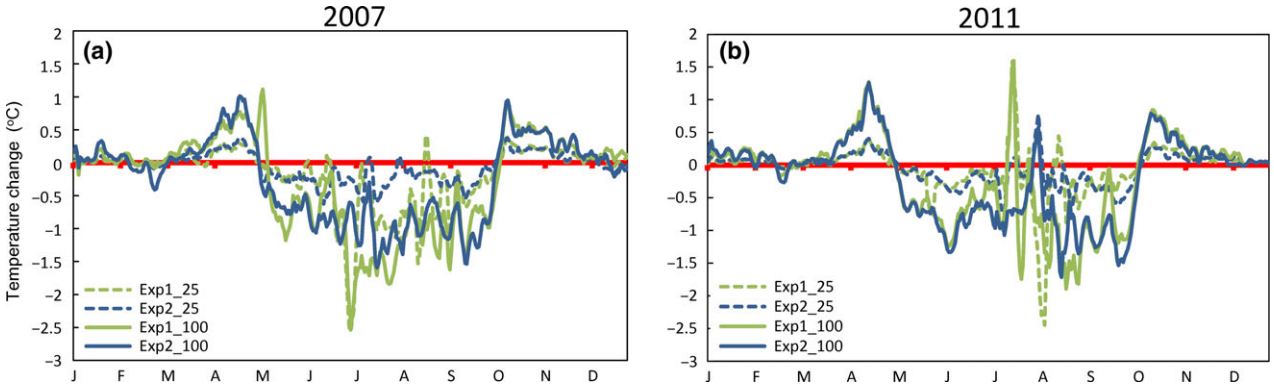

Fig. 7 Domain-averaged time series of temperature differences between perennial biofuel crop and control for (a) 2007 and (b) 2011. Green and blue lines represent Exp1 (best skilled control simulation) and Exp2 (least skilled control simulation), respectively. Dashed and solid lines represent 25% and 100% perennial biofuel deployment scenarios, respectively.

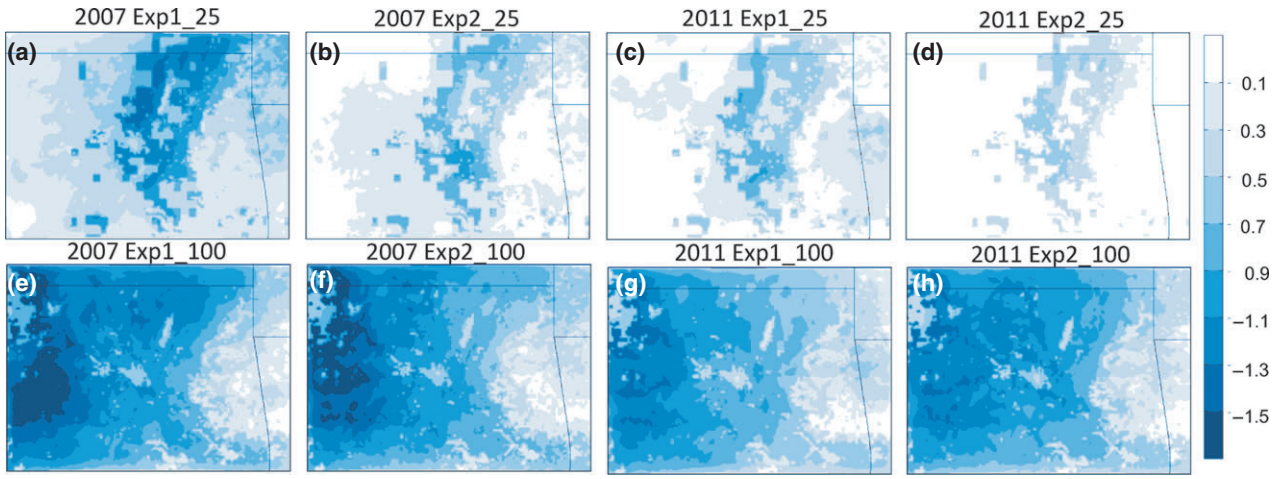

Fig. 8 Mean temperature differences (average of May-October) between perennial biofuel crop deployment experiments and control experiments for Exp1_25 and Exp2_25 for the years 2007 (a, b) and 2011 (c, d) and Exp1_100 and Exp2_100 deployment for the years 2007 (e, f) and 2011 (g, h).

precipitation results (Table S1) unlike ET. Further examination of thermodynamic impacts, as drivers of simulated precipitation, is necessary. Simulated differences were also evident in 2011, although of reduced magnitude, as ET increases from July to September varied among experiments, pointing to issues of model performance. Outside of the summer months, the simulated effects of ET associated with perennial biofuel crops generally followed similar patterns for both years: a decrease in ET of about 1 mm day^{-1} from April to May and a smaller decrease (~0.5 mm day^{-1}) from October to November (likely driven by greater LAI and vegetation fraction for simulations using default biophysical characteristics relative to bioenergy cropping simulations). The decrease from April to May was more pronounced in 2011, with ET values approximately 38% lower than those in 2007.

In addition to experimental sensitivity, annual differences in simulated ET impacts from perennial biofuel crop deployment were also apparent between normal hydrometeorological (2007) and drought (2011) years. Simulated ET impacts associated with perennial bioenergy crop deployment were moderated during the drought year relative to the normal climate year. Focusing on Exp1 (the best skilled ensemble member), ET associated with perennial biofuel crop deployment was 37% lower, on average, during the growing season in 2011 relative to 2007 (0.28 mm day^{-1} compared with 0.44 mm day^{-1}, respectively). This decrease was even more pronounced from July to September, as ET associated with perennial biofuel crop deployment was 3.4 times lower in 2011 relative to 2007 (0.21 mm day^{-1} compared with 0.73 mm day^{-1}). During the summer of 2011, ET decreased from June to July for both Exp1 and

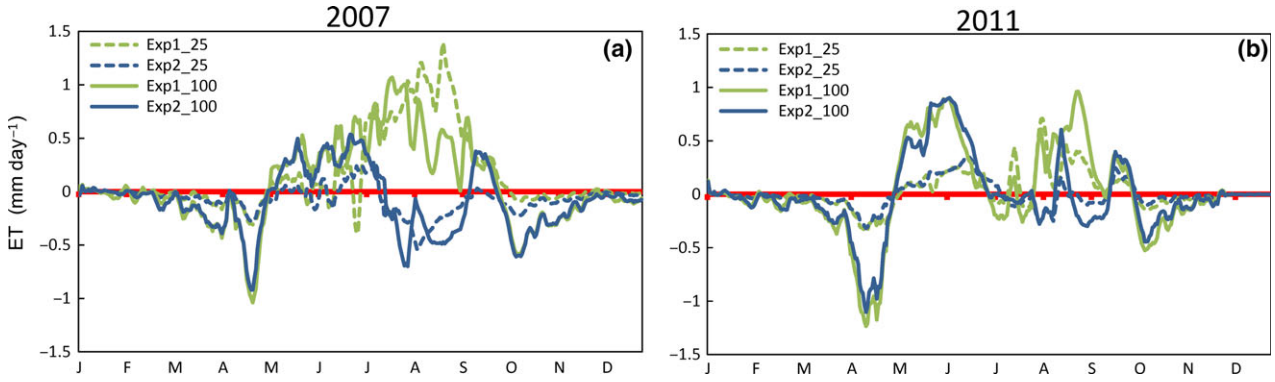

Fig. 9 Domain-averaged time series of evapotranspiration (ET) differences between perennial biofuel crop deployment experiments and control experiments for (a) 2007 and (b) 2011. Panel representation is the same as in Fig. 7.

2 and then remained just below zero for most of July to August. Despite this decrease, ET was enhanced under perennial biofuel crop deployment by an average of 0.25 mm day^{-1} and 0.13 mm day^{-1} over the growing season for Exp1 and 2, respectively, indicating the potential to mitigate the effects of drought through the enhanced ET.

Soil moisture impacts associated with perennial biofuel crop deployment followed the seasonal patterns of withdrawal and recharge based on crop phenology and atmospheric processes. The domain-averaged evolution of soil moisture associated with perennial biofuel crop deployment demonstrated the depletion from May through August, followed by a recharge period in the fall and winter due to the increased large-scale precipitation activity. After the growing season, soil moisture was restored near the surface, but remained partially depleted at rooting depths, 10–40 cm and 40 cm–1 m (Fig. 10). These deficits were most noticeable at rooting depth 40 cm–1 m, as the amount of soil moisture was 20% and 10% less than their initial state in 2007 and 2011, respectively (Fig. 10c, f). Other annual differences were also apparent from April to May, as soil moisture was approximately 29% lower in 2011 than in 2007 (Fig. 10c, f). In addition to annual differences, Exp2 resulted in lower soil moisture than Exp1 at all rooting depths with the largest disparities during 2007 (Fig. 10a–c). Moreover, at the beginning of the year, Exp1 noted almost 20% higher soil moisture in 2007 near the surface and 10–40 cm. Experimental differences in soil moisture amounts were attenuated in 2011 relative to 2007, pointing to less water uptake associated with these cropping systems under drier hydrometeorological conditions. Lastly, different deployment scenarios also affected the amount of soil moisture depletion with slightly higher withdrawals associated with full deployment scenario, especially during 2011.

Mechanisms driving simulated changes

The principle processes driving the aforementioned impacts are grounded on the changes in the radiation budget. During the growing season, the net shortwave radiation associated with perennial biofuel crop deployment decreased by an average of 15.8 W m^{-2}, while net longwave radiation associated with perennial biofuel crop deployment increased by an average of 5.6 W m^{-2}, for both years (Fig. 11). Only minor differences were discernible between years for perennial bioenergy crop deployment with slightly higher net shortwave radiation values in 2007 and slightly higher net longwave radiation in 2011. Larger differences existed between deployment scenarios. Under full deployment scenarios, the decrease in net shortwave radiation was on average 14.5 W m^{-2} greater (Fig. 11a, b), while net longwave radiation fluxes were only 4.3 W m^{-2} higher on average relative to partial deployment scenarios (Fig. 11c, d). Additionally, Fig. 11c, d shows decreases in net longwave radiation associated with perennial bioenergy crop deployment from April to May and October to November, which correlated with temperature decreases in the previously presented time-series analysis (see Fig. 7). This decrease was more pronounced in the spring of both years by an average of 10 W m^{-2}, but even more so in 2011, and is driven by the imposed, observationally based, biogeophysical representation of perennial crops.

Simulated energy fluxes associated with perennial bioenergy crop deployment illustrate the diverging results for both sensible and latent heat fluxes based on model performance and climate year, similar to ET (Fig. 12). Model simulation results for both sensible and latent heat fluxes show a diverging evolution between Exp1 and Exp2 from July to September 2007 (Fig. 12a, c). Despite the experimental differences, both Exp1 and Exp2 pointed to increasing latent heat fluxes and

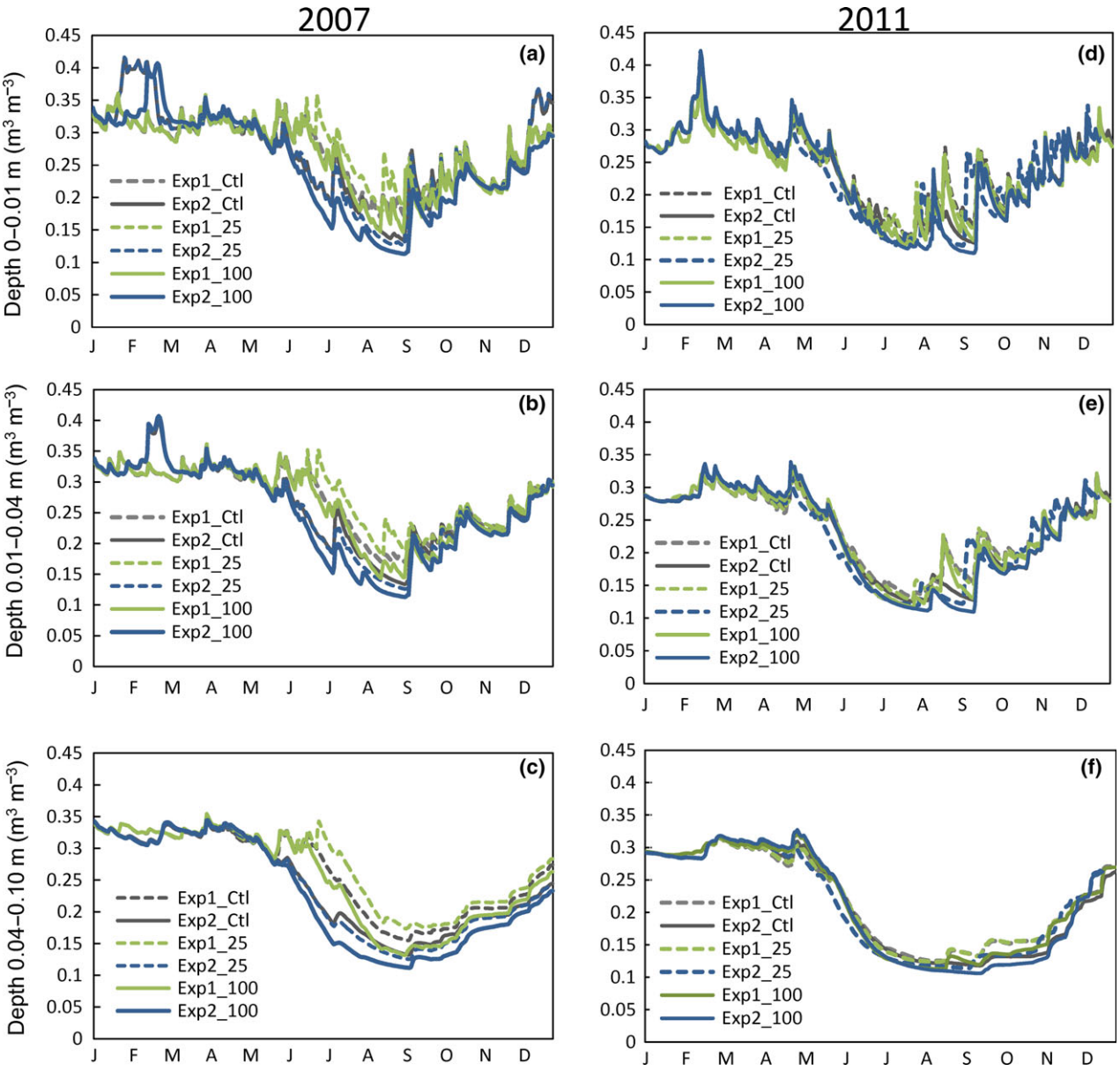

Fig. 10 Domain-averaged time series of soil moisture at model depths 0–0.01, 0.01–0.04, and 0.04–0.10 meters (from top to bottom). Figures (a–c) and (d–f) correspond to the years 2007 and 2011, respectively. Gray, green, and blue lines represent control, Exp1, and Exp2, respectively. Dashed and solid lines represent 25% and 100% perennial biofuel deployment scenarios, respectively.

decreasing sensible heat fluxes associated with perennial bioenergy crop deployment during the growing season. In 2007, energy flux differences associated with perennial bioenergy crops were most distinctive under the full deployment scenario, varying by 30–40 W m^{-2} from July to September. In 2011, these differences were moderated as both sensible and latent heat fluxes varied 10–20 W m^{-2}. Outside of the growing season, changes in energy fluxes associated with perennial bioenergy crop deployment were also apparent mainly from April to May, with spikes in sensible heat and commensurate declines in latent heat fluxes (Fig. 12). These changes were most noticeable with latent heat fluxes especially in 2011 (Fig. 12a, b), which also correlated with temperature and radiation flux differences.

Because the largest simulated effects on energy fluxes were most apparent during the growing season, we examined the spatial effects of energy fluxes associated with perennial bioenergy crop deployment from May to October. During the growing season, latent heat fluxes increased (Fig. 13a–h), while sensible heat fluxes decreased (Fig. 13i–p). Energy flux differences were

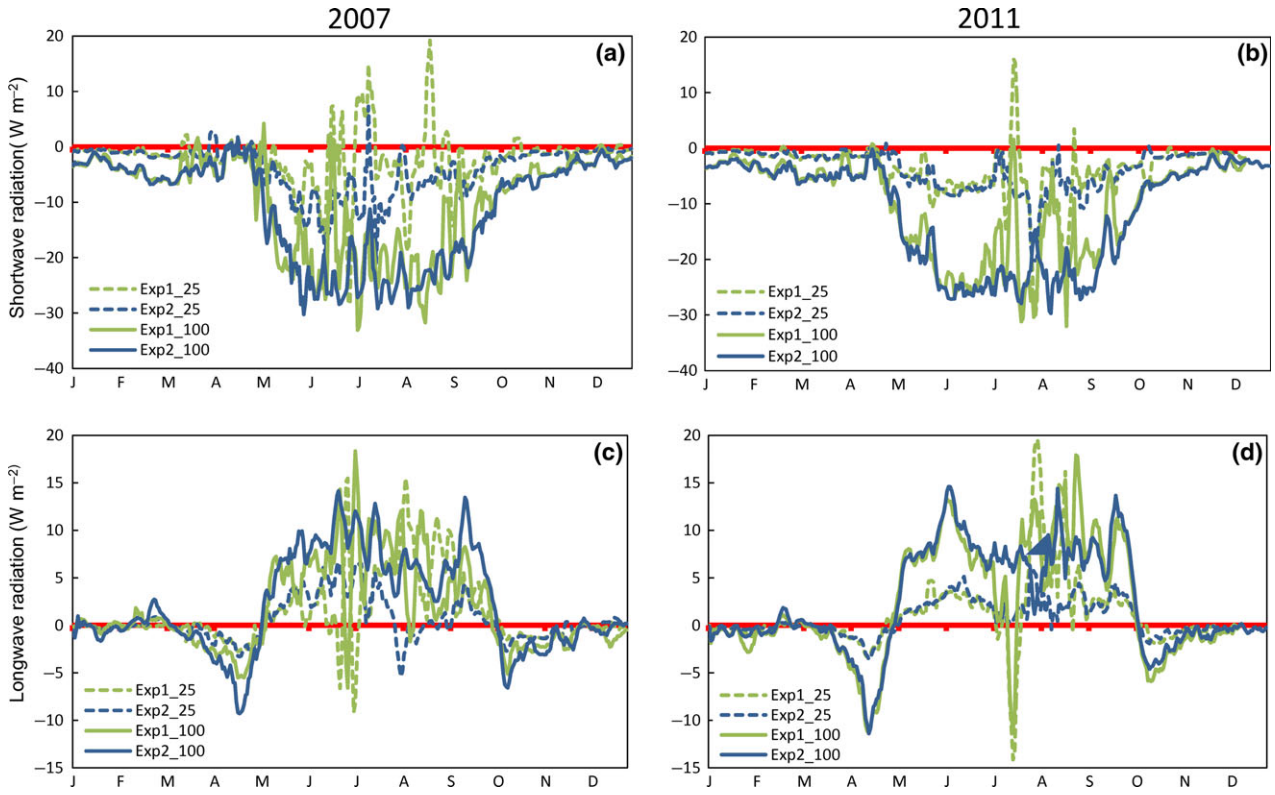

Fig. 11 Domain-averaged time series of net shortwave radiation differences between perennial biofuel crop experiments and control experiments for the years (a) 2007 and (b) 2011 and the net longwave radiation differences for the years (c) 2007 and (d) 2011. Panel representation is the same as in Fig. 7.

most noticeable under the full deployment compared with the partial deployment scenarios, with the exception of Exp1_25 and Exp1_100 in 2007 (Fig. 13b, d, j, l). For these two experiments, sensible heat fluxes increased in the eastern part of the domain (Fig. 13d), which correlated with a decrease in latent heat fluxes (Fig. 13l). Despite this anomaly, both latent and sensible heat fluxes exhibited a west-to-east gradient under full deployment scenario with the highest flux differences located in the west, coincident with the spatial pattern of temperature differences. Energy flux differences were more localized under the partial deployment compared with the full deployment scenario, despite the increases in latent heat and the decreases in sensible heat fluxes observed beyond the deployment areas.

Contrasting different hydrometeorological years, changes in sensible and latent heat fluxes associated with perennial bioenergy crop deployment were moderated in 2011 relative to 2007. In 2007, latent heat fluxes increased up to 50 W m^{-2}, while sensible heat fluxes decreased up to 50 W m^{-2}. In 2011, latent heat flux increases were approximately 10–25 W m^{-2} lower relative to 2007 and covered a smaller portion of the domain. Sensible heat fluxes followed a similar pattern with moderated decreases in 2011. This attenuation of energy flux differences was most distinctive with Exp2 and the partial deployment scenario, indicating the sensitivity to model performance and the availability of atmospheric moisture.

Discussion and conclusions

This study examined the hydrometeorological impacts of perennial biofuel crop expansion using varying realistic deployment scenarios [i.e., partial deployment (14 376.3 square kilometers) and full deployment (56 667.2 square kilometers)] under diverse hydrometeorological conditions [i.e., drought year (2011) and normal year (2007)]. We focus bioenergy deployment only within suitable marginal and abandoned lands (see Cai *et al.*, 2010). Our analyses show that perennial bioenergy crop deployment leads to the widespread cooling (1–2 °C) and the enhanced ET (0.5–1.0 mm day^{-1}) during the growing season – May to October (see Figs 7 and 9). In this study, soil moisture was depleted from mid-May to mid-August contributing to the enhanced ET, but nearly restored during senescence (mid-August to December) (see Fig. 10). The amount of soil moisture depletion was 20% and 10% less than the initial state in 2007 and 2011, respectively, and largely a function of

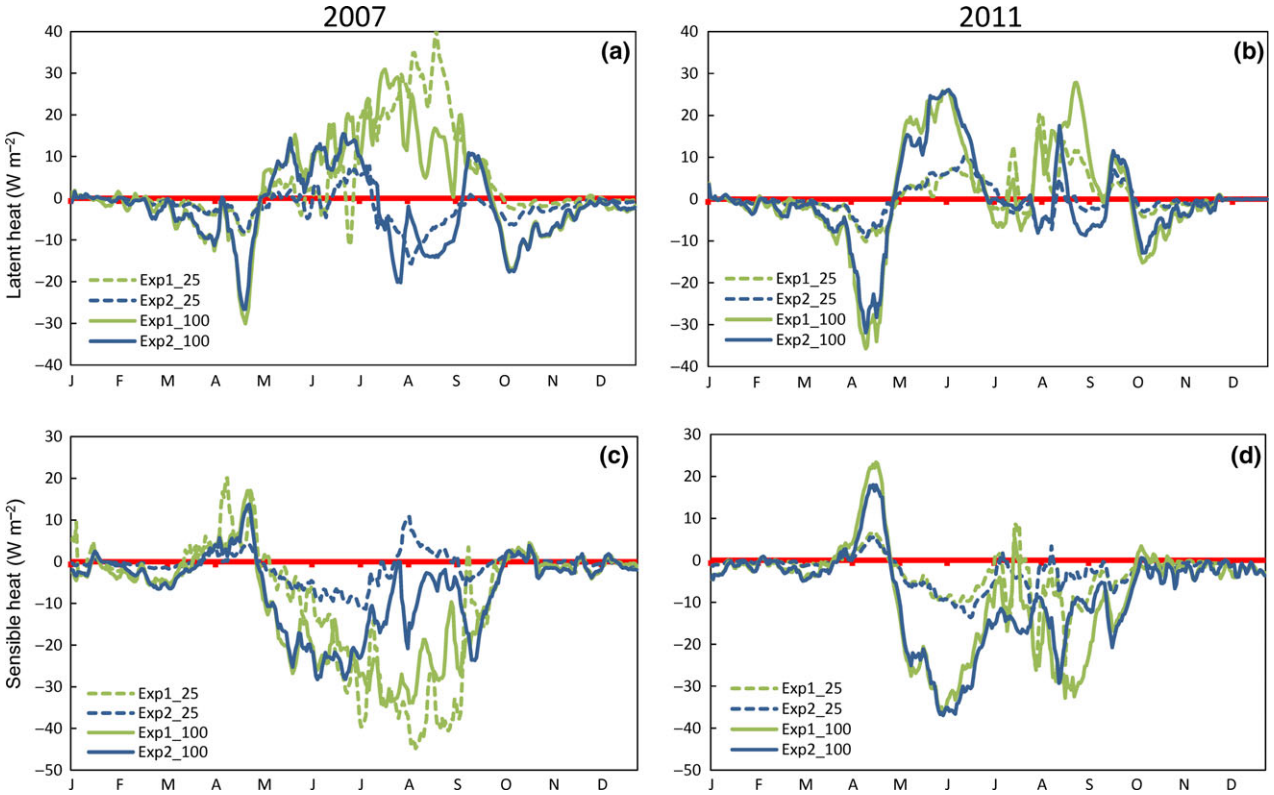

Fig. 12 Domain-averaged time series of latent heat fluxes differences between perennial biofuel crop experiments and control experiments for the years (a) 2007 and (b) 2011 and sensible heat fluxes differences for the years (c) 2007 and (d) 2011. Panel representation is the same as in Fig. 7.

moisture availability tied to hydrometeorological conditions. These hydrometeorological impacts were more evident under the full deployment, but still detectable within the deployment areas under the partial deployment scenario as well as in the surrounding environment. This finding indicates that perennial biofuel crops could still have important hydroclimate implications, even with small-scale distribution.

During the growing season, perennial bioenergy crops have higher LAI, albedo, and vegetation fraction values compared with existing grasslands (see Fig. 3). These physiological differences resulted in near-surface cooling and enhanced ET, in agreement with the findings of previous studies (Georgescu *et al.*, 2009, 2011; Hickman *et al.*, 2010; McIsaac *et al.*, 2010; Vanloocke *et al.*, 2010; Zeri *et al.*, 2013; Miller *et al.*, 2015; Zhu *et al.*, 2016). Higher albedo values, however, proved to be the dominant mechanism for these simulated impacts through the subsequent decrease in absorbed surface shortwave radiation resulting in cooler temperatures. Previous studies attributed regional cooling, in part, to the enhanced ET from the dense and deep rooting systems of perennial bioenergy crops drawing down soil moisture at deeper soil depths (Clifton-Brown *et al.*, 2007; Vanloocke *et al.*, 2010; Georgescu *et al.*, 2011; Anderson *et al.*, 2013; Hallgren *et al.*, 2013; Ferchaud *et al.*, 2015). While physiological or morphological factors (i.e., LAI and vegetation fraction) can alter the surface energy balance and enhance ET during green-up, hydrometeorological impacts could primarily be a function of radiative forcing, as indicated here, because the rooting systems of perennial biofuel crops and existing grasslands were characteristically similar and therefore unaltered in this study.

This study also examined whether perennial biofuel crop expansion could ameliorate drought conditions by contrasting the potential hydroclimate impacts of perennial biofuel crops during a drought year (2011) and normal year (2007). Our analyses show that perennial bioenergy crop deployment reduced the impacts of drought through the enhanced ET and simultaneously cooling of the near-surface environment, by decreasing the atmospheric demand for water (Seneviratne *et al.*, 2010) and mitigating plant stress due to water availability (Wu *et al.*, 2002). During the growing season, near-surface cooling and enhanced ET associated with these crops were moderated under the drought year relative to the normal climate year due to the moisture

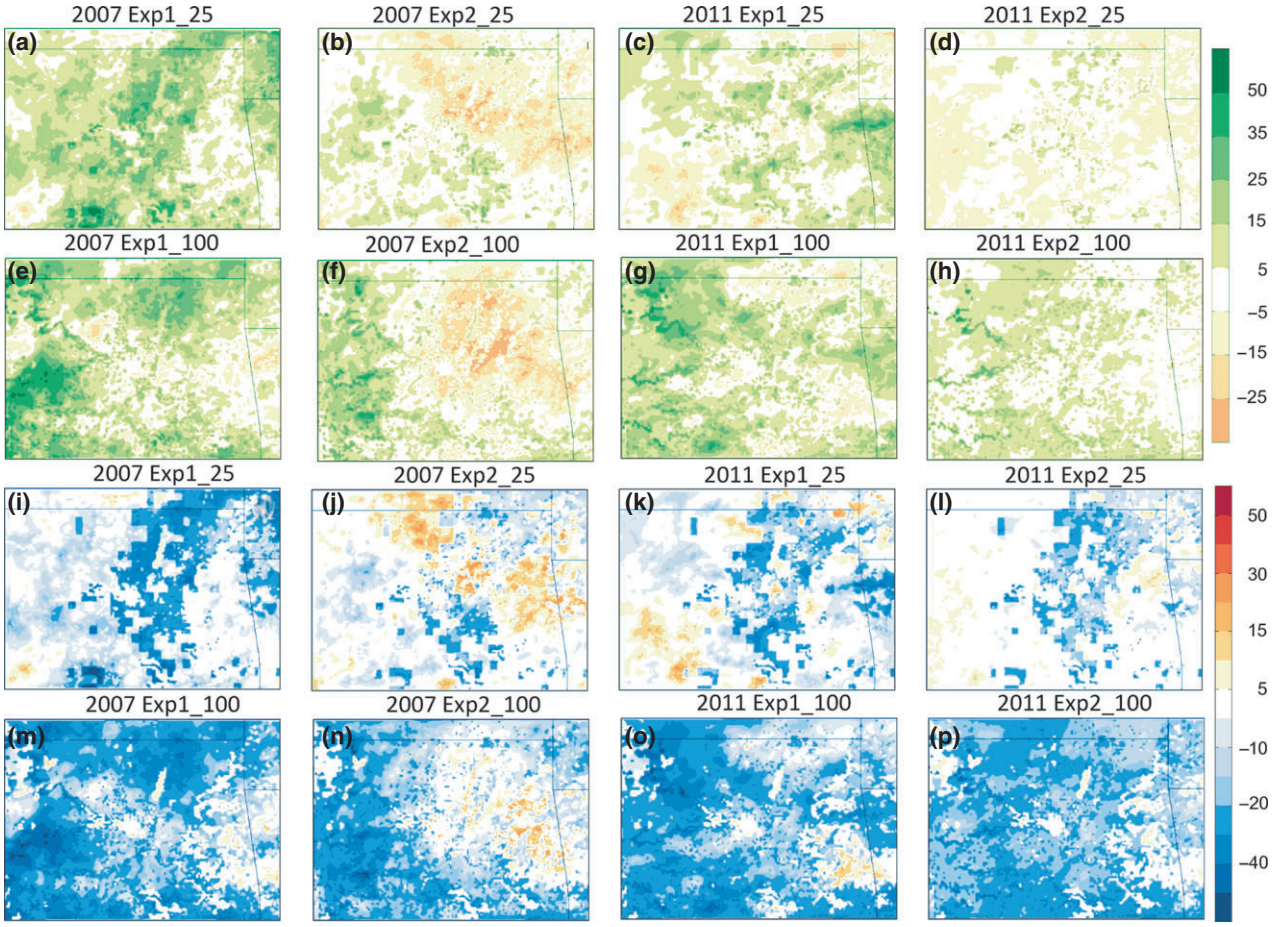

Fig. 13 Mean latent flux differences (average of May–October) between perennial biofuel crop experiments and control experiments for Exp1-2 (from left to right) 25% deployment for the year 2007. Figures (a, b) and 2011 (c, d) and 100% deployment for the years 2007 Figures (e, f) and 2011 (g, h) and sensible heat fluxes 25% deployment for the years 2007 Figures (i, j) and 2011 (k, l) and 100% deployment for the year 2007. Figures (m, n) and 2011 (o, p).

availability and the subsequent alterations in near-surface radiation and energy budgets. These changes revealed the differential effects of simulated perennial bioenergy crop impacts based on background environmental conditions. Despite the moderation of these hydrometeorological impacts, perennial biofuel crop expansion was shown to mitigate the impacts of drought (i.e., via an increased ET) and can potentially serve as a more sustainable pathway to renewable energy than current strategies given these additional unintended, but positive, consequences. The length of timescale perturbations associated with these cropping systems, however, must be considered as the small, and negative feedback of soil moisture depletion could amplify drought severity under a multiyear drought scenario. Therefore, additional multiyear high-resolution simulations are necessary to definitively conclude whether such approaches could simultaneously provide the biomass necessary for ethanol production while ameliorating large-scale climate change through the alteration of near-surface regional climate.

It is important to note that further hydroclimate impacts were observed from April to May and October to November outside the 'active' growing season. During these periods, perennial bioenergy crop expansion points to warmer near-surface temperatures and decreased ET. These hydrometeorological impacts were more prominent during the green-up period than during the senescence. Vegetation fraction values were significantly higher than albedo and LAI for existing grasslands relative to perennial bioenergy crops during this green-up period (see Fig. 3a). This difference could be an artifact of how vegetation fraction values were scaled. It is possible that vegetation fraction evolution could progress more slowly during the spring and late fall, but requires field observation data that were unavailable (Wagle *et al.*, 2016). Other factors such as soil moisture availability and litter layer thickness could

have contributed to these decreases in longwave radiation and latent heat fluxes from April to May 2011 as soil moisture levels were approximately 29% lower in 2011 relative to 2007 (see Fig. 8a–f).

Sensitivity to bioenergy crop deployment was largely independent of control simulation skill for thermal impacts, but proved to be a determining factor for simulated ET. Experimental differences were in good agreement on the simulated thermal impacts of perennial bioenergy crops as temperature decreases were generally within 0.2 °C (Fig. 7) and spatially consistent between Exp1 (the best skilled ensemble member) and Exp2 (the least skilled ensemble member). Unlike temperature, simulated ET impacts associated with perennial bioenergy crops diverged, mainly during July to September 2007. During this period, Exp1 showed that ET increased on average by 0.73 mm day^{-1}, while Exp2 showed that ET decreased by an average of 0.19 mm day^{-1}. Other experimental differences were evident in 2011 as ET increases varied according to model solution from July to September, pointing to issues of model performance and simulated atmospheric processes (see Fig. 9). During the growing season, Exp1 consistently displayed higher ET, latent heat fluxes, and soil moisture relative to Exp2, especially during 2007. Although both experiments noted a dry bias in model evaluation (see Fig. 6a, f, i, n), Exp2 significantly underestimated the amount of precipitation, most likely as a result of microphysics scheme selection (see Table 3). This dry bias associated with Exp2 could explain the significantly lower latent heat fluxes, lower soil moisture levels, and higher sensible heat fluxes, affecting simulated ET associated with perennial bioenergy crop expansion.

Simulated impacts of precipitation associated with perennial biofuel crop deployment also highlighted the sensitivity of control simulation skill, but are characterized as lower confidence relative to the aforementioned impacts. For both years, the simulated precipitation pointed to a positive signal under Exp1, while the simulated precipitation indicated a negative signal under Exp2, likely indicative of the dry bias associated with Exp2 (see Fig. S1 and Table S1). Similar to the simulated ET and latent heat flux, precipitation totals were attenuated during the drought year relative to normal climate year, pointing to moisture availability tied to hydrometeorological conditions. Unlike the aforementioned impacts, the simulated precipitation totals were also reduced under the full deployment relative to the partial deployment scenario, even during the normal climate year. This finding points to radiative forcing as the driving mechanism for simulated results, as decreased low-level heating resulting from reduced shortwave absorption lowers the available energy necessary for convection and, consequently, the amount of precipitation (Findell & Elathir, 2003; Seneviratne *et al*., 2010). This mechanism, however, requires further examination focusing exclusively on the untangling of disparate forcing mechanisms owing to differential background dynamics at different times of year and is beyond the scope of this manuscript.

The use of a singular LSM, rather than a suite of models with diverse physiological representations of plant functional types and physical representations of land surface flux energy partitioning, is a necessary area for future research. For example, simulated canopy temperature and associated surface fluxes, which regulate the regional hydrologic cycle, are not resolved separately in NOAH, but rather are calculated over a combined surface of vegetation and soil (Niu *et al*., 2011). This important point emphasizes the need for utility of a fully coupled earth system model that includes a dynamically evolving biophysical representation of perennial bioenergy cropping systems, such as the community land model (Zeng *et al*., 2002). Such an effort will improve upon the physiological characterization of the investigated plant type, which is dependent on ambient environmental conditions rather than on the presumed periodic depiction utilized here. In effect, imposed energy crop biophysical characteristics may be different under a drought compared with a normal precipitation year. Finally, the impacts on groundwater require examination using appropriate models that account for such hydrologic elements (e.g., NOAH-MP and LEAF-2 dynamically coupled to WRF [e.g., Miguez-Macho *et al*., 2007)].

Future work should also assess the hydrometeorological impacts of perennial biofuel crops using high-resolution simulations in other geographical regions to evaluate the range of potential outcomes with this energy pathway. Yield estimates should also be calculated to provide information on how diverse hydrometeorological conditions could potentially affect bioenergy crop yields by using an ecosystem model such as Agro-IBIS (e.g., Vanloocke *et al*., 2010). Long-term, continuous climate simulations of perennial biofuel crop expansion are also needed to understand the resiliency of these cropping systems under a variable current climate and under projected warmer climates associated with higher levels of greenhouse gas emissions. Varying aspects of this work are underway.

Acknowledgement

This work was funded by NSF Grant EAR-1204774.

References

Abatzoglou JT (2013) Development of gridded surface meteorological data for ecological applications and modelling. *International Journal of Climatology*, **33**, 121–131.

Abraha M, Chen J, Chu H *et al.* (2015) Evapotranspiration of annual and perennial biofuel crops in a variable climate. *GCB Bioenergy*, **7**, 1344–1356.

Anderson CJ, Anex RP, Arritt RW, Gelder BK, Khanal S, Herzmann DE, Gassman PW (2013) Regional climate impacts of a biofuels policy projection. *Geophysical Research Letters*, **40**, 1217–1222.

Anderson-Teixeira KJ, Snyder PK, Twine TE, Cuadra SV, Costa MH, DeLucia EH (2012) Climate-regulation services of natural and agricultural ecoregions of the Americas. *Nature Climate Change*, **2.3**, 177–181.

Bagley JE, Davis SC, Georgescu M *et al.* (2014) The biophysical link between climate, water, and vegetation in bioenergy agro-ecosystems. *Biomass and Bioenergy*, **71**, 187–201.

Bagley JE, Miller J, Bernacchi CJ (2015) Biophysical impacts of climate-smart agriculture in the Midwest United States. *Plant, Cell, and Environment*, **38**, 1913–1930.

Bright RM, Cherubini F, Strømman AH (2012) Climate impacts of bioenergy: inclusion of carbon cycle and albedo dynamics in life cycle impact assessment. *Environmental Impact Assessment Review*, **37**, 2–11.

Bright RM, Bogren W, Bernier P, Astrup R (2016) Carbon-equivalent metrics for albedo changes in land management contexts: relevance of the time dimension. *Ecological Applications*, **26**, 1868–1880.

Cai X, Zhang X, Wang D (2010) Land availability for biofuel production. *Environmental Science and Technology*, **45**, 334–339.

Campbell JE, Lobell DB, Genova RC, Field CB (2008) The global potential of bioenergy on abandoned agriculture lands. *Environmental Science and Technology*, **42**, 5791–5794.

Campbell JE, Lobell DB, Genova RC, Zumkehr A, Field CB (2013) Seasonal energy storage using bioenergy production from abandoned croplands. *Environmental Research Letters*, **8**, 035012.

Cao Q, Yu D, Georgescu M, Han Z, Wu J (2015) Impacts of land use and land cover change on regional climate: a case study in the agro-pastoral transitional zone of China. *Environmental Research Letters*, **10**, 124025.

Chen G, Zhao L, Qi Y (2015) Enhancing the productivity of microalgae cultivated in wastewater toward biofuel production: a critical review. *Applied Energy*, **137**, 282–291.

Clifton-Brown JC, Breuer J, Jones MB (2007) Carbon mitigation by the energy crop, Miscanthus. *Global Change Biology*, **13**, 2296–2307.

Davis AS, Hill JD, Chase CA, Johanns AM, Liebman M (2012) Increasing cropping system diversity balances productivity, profitability and environmental health. *PLoS ONE*, **7**, e47149.

Devaraju N, Bala G, Nemani R (2015) Modelling the influence of land-use changes on biophysical and biochemical interactions at regional and global scales. *Plant, Cell & Environment*, **38**, 1931–1946.

Ek MB, Mitchell KE, Lin Y, et al. (2003) Implementation of Noah land surface model advances in the National Centers for Environmental Prediction operational mesoscale Eta model. *Journal of Geophysical Research: Atmospheres*, **108**, (D22) 8851. doi:10.1029/2002JD003296.

Feng Q, Chaubey I, Her YG, Cibin R, Engel B, Volenec J, Wang X (2015) Hydrologic and water quality impacts and biomass production potential on marginal land. *Environmental Modelling and Software*, **72**, 230–238.

Ferchaud F, Vitte G, Bornet F, Strullu L, Mary B (2015) Soil water uptake and root distribution of different perennial and annual bioenergy crops. *Plant and Soil*, **388**, 307–322.

Findell KL, Eltahir EA (2003) Atmospheric controls on soil moisture-boundary layer interactions. Part I: framework development. *Journal of Hydrometeorology*, **4**, 552–569.

Foley JA, DeFries R, Asner GP *et al.* (2005) Global consequences of land use. *Science*, **309**, 570–574.

Gelfand I, Sahajpal R, Zhang X, Izaurralde RC, Gross KL, Robertson GP (2013) Sustainable bioenergy production from marginal lands in the US Midwest. *Nature*, **493**, 514–517.

Georgescu M, Lobell DB, Field CB (2009) Potential impact of US biofuels on regional climate. *Geophysical Research Letters*, **36**, L21806.

Georgescu M and Lobell DB (2010) Perennial questions of hydrology and climate. *Science*, **330**(1), 33.

Georgescu M, Lobell DB, Field CB (2011) Direct climate effects of perennial bioenergy crops in the United States. *Proceedings of the National Academy of Sciences*, **108**, 4307–4312.

Georgescu M, Lobell DB, Field CB Mahalov A(2013) Simulated hydroclimatic impacts of projected Brazilian sugarcane expansion. *Geophysical Research Letters*, **40**, 972–977.

Goldstein JC, Tarhule A, Brauer D (2014) Simulating the hydrologic response of a semiarid watershed to switchgrass cultivation. *Hydrology Research*, **45**, 99–114.

Gopalakrishnan G, Negri C, Salas W (2012) Modeling biogeochemical impacts of bioenergy buffers with perennial grasses for a row-crop field in Illinois. *GCB Bioenergy*, **4**, 739–750.

Haberl H, Beringer T, Bhattacharya SC, Erb KH, Hoogwijk M (2010) The global technical potential of bio-energy in 2050 considering sustainability constraints. *Current Opinion in Environmental Sustainability*, **2**, 394–403.

Hallgren W, Schlosser CA, Monier E, Kicklighter D, Sokolov A, Melillo J (2013) Climate impacts of a large-scale biofuels expansion. *Geophysical Research Letters*, **40**, 1624–1630.

Hickman GC, Vanloocke A, Dohleman FG, Bernacchi CJ (2010) A comparison of canopy evapotranspiration for maize and two perennial grasses identified as potential bioenergy crops. *GCB Bioenergy*, **2**, 157–168.

Hoerling M, Kumar A, Dole R *et al.* (2013) Anatomy of an extreme event. *Journal of Climate*, **26**, 2811–2832.

Hudiburg TW, Davis SC, Parton W, Delucia EH (2015) Bioenergy crop greenhouse gas mitigation potential under a range of management practices. *GCB Bioenergy*, **7**, 366–374.

Hudiburg TW, Wang W, Khanna M *et al.* (2016) Impacts of a 32-billion-gallon bioenergy landscape on land and fossil fuel use in the US. *Nature Energy*, **1**, 15005.

Joo E, Hussain MZ, Zeri M *et al.* (2016) The influence of drought and heat stress on long term carbon fluxes of bioenergy crops grown in the Midwestern US. *Plant, Cell and Environment*, **39**, 1928–1940.

Khanal S, Anex RP, Anderson CJ, Herzmann DE, Jha MK (2013) Implications of biofuel policy-driven land cover change for rainfall erosivity and soil erosion in the United States. *GCB Bioenergy*, **5**, 713–722.

Khanal S, Anex RP, Anderson CJ, Herzmann DE (2014) Streamflow impacts of biofuel policy-driven landscape change. *PLoS ONE*, **9**, e109129.

Le PV, Kumar P, Drewry DT (2011) Implications for the hydrologic cycle under climate change due to the expansion of bioenergy crops in the Midwestern United States. *Proceedings of the National Academy of Sciences*, **108**, 15085–15090.

López-Bellido L, Wery J, López-Bellido RJ (2014) Energy crops: prospects in the context of sustainable agriculture. *European Journal of Agronomy*, **60**, 1–12.

McIsaac GF, David MB, Mitchell CA (2010) Miscanthus and switchgrass production in Central Illinois: impacts on hydrology and inorganic nitrogen leaching. *Journal of Environmental Quality*, **39**, 1790–1799.

Melillo JM, Reilly JM, Kicklighter DW *et al.* (2009) Indirect emissions from biofuels: how important?. *Science*, **326**, 1397–1399.

Miguez-Macho G, Fan Y, Weaver CP, Walko R, Robock A (2007) Incorporating water table dynamics in climate modeling: 2. Formulation, validation, and soil moisture simulation. *Journal of Geophysical Research: Atmospheres*, **112**, D13108. doi:10.1029/2006JD008112

Miller JN, VanLoocke A, Gomez-Casanovas N, Bernacchi CJ (2015) Candidate perennial bioenergy grasses have a higher albedo than annual row crops in the Midwestern US. *Global Change Biology*, **21**, 4237–4249.

Niu GY, Yang ZL, Mitchell KE *et al.* (2011) The community Noah land surface model with multiparameterization options (Noah MP): 1. Model description and evaluation with local scale measurements. *Journal of Geophysical Research: Atmospheres*, **116**, D12109. doi:10.1029/2010JD015139

Oikawa PY, Jenerette GD, Grantz DA (2015) Offsetting high water demands with high productivity: sorghum as a biofuel crop in a high irradiance arid ecosystem. *GCB Bioenergy*, **7**, 974–983.

Pielke RA (2001) Influence of the spatial distribution of vegetation and soils on the prediction of cumulus convective rainfall. *Reviews of Geophysics*, **39**, 151–177.

Pielke RA (2005) Land use and climate change. *Science*, **310**, 1625–1626.

Rahman MM, Mostafiz SB, Paatero JV, Lahdelma R (2014) Extension of energy crops on surplus agricultural lands: a potentially viable option in developing countries while fossil fuel reserves are diminishing. *Renewable and Sustainable Energy Reviews*, **29**, 108–119.

RFA (Renewable Fuel Association) (2010) Statistics, Annual World Ethanol Production by Country (based on F.O. Licht estimates). Available at: http://www.ethanolrfa.org/pages/statistics#E (accessed 26 October 2010).

Seneviratne SI, Corti T, Davin EL *et al.* (2010) Investigating soil moisture–climate interactions in a changing climate: a review. *Earth-Science Reviews*, **99**, 125–161.

Skamarock WC, Klemp JB, Dudhia J, Gill DO, Barker DM, Wang W, Powers JG (2005) *A description of the advanced research WRF version 2* (No. NCAR/TN-468+STR). National Center For Atmospheric Research Boulder Co Mesoscale and Microscale Meteorology Div.

Tadesse T, Wardlow BD, Brown JF, Svoboda MD, Hayes MJ, Fuchs B, Gutzmer D (2015) Assessing the vegetation condition impacts of the 2011 drought across the US southern great plains using the vegetation drought response index (VegDRI). *Journal of Applied Meteorology and Climatology*, **54**, 153–169.

Taylor KE (2001) Summarizing multiple aspects of model performance in a single diagram. *Journal of Geophysical Research: Atmospheres*, **106**, 7183–7192.

United States Drought Monitor (2014). Available at: http://droughtmonitor.unl.edu/MapsAndData/GISData.aspx (accessed 16 October 2014)

Vanloocke A, Bernacchi CJ, Twine TE (2010) The impacts of Miscanthus× giganteus production on the Midwest US hydrologic cycle. *GCB Bioenergy*, **2**, 180–191.

VanLoocke A, Twine TE, Kucharik CJ, Bernacchi CJ (2016) Assessing the potential to decrease the Gulf of Mexico hypoxic zone with Midwest US perennial cellulosic feedstock production. *GCB Bioenergy*, **9**, 858–875.

Wagle P, Kakani VG (2014) Seasonal variability in net ecosystem carbon dioxide exchange over a young Switchgrass stand. *GCB Bioenergy*, **6**, 339–350.

Wagle P, Kakani VG, Huhnke RL (2016) Evapotranspiration and ecosystem water use efficiency of switchgrass and high biomass sorghum. *Agronomy Journal*, **108**, 1007–1019.

Weaver CP, Avissar R (2001) Atmospheric disturbances caused by human modification of the landscape. *Bulletin of the American Meteorological Society*, **82**, 269–281.

Wu W, Geller MA, Dickinson RE (2002) The response of soil moisture to long-term variability of precipitation. *Journal of Hydrometeorology*, **3**, 604–613.

Xu X, Scanlon BR, Schilling K, Sun A (2013) Relative importance of climate and land surface changes on hydrologic changes in the US Midwest since the 1930s: implications for biofuel production. *Journal of Hydrology*, **497**, 110–120.

Yimam YT, Ochsner TE, Kakani VG (2015) Evapotranspiration partitioning and water use efficiency of switchgrass and biomass sorghum managed for biofuel. *Agricultural Water Management*, **155**, 40–47.

Zeng X, Shaikh M, Dai Y, Dickinson RE, Myneni R (2002) Coupling of the common land model to the NCAR community climate model. *Journal of Climate*, **15**, 1832–1854.

Zeri M, Hussain MZ, Anderson-Teixeira KJ, DeLucia E, Bernacchi CJ (2013) Water use efficiency of perennial and annual bioenergy crops in central Illinois. *Journal of Geophysical Research: Biogeosciences*, **118**, 581–589.

Zhu P, Zhuang Q, Joo E, Bernacchi C (2016) Importance of biophysical effects on climate warming mitigation potential of biofuel crops over the conterminous United States. *GCB Bioenergy*, **9**, 577–590.

Zumkehr A, Campbell JE (2013) Historical US cropland areas and the potential for bioenergy production on abandoned croplands. *Environmental Science and Technology*, **47**, 3840–3847.

Supporting Information

Additional Supporting Information may be found online in the supporting information tab for this article:

Figure S1 Total precipitation differences (totals from May-October) between perennial biofuel crop deployment experiments and Control experiments for Exp1_25 and Exp2_25 for the years of 2007 (a, b) and 2011 (c, d), and Exp1_100 and Exp2_100 deployment for the years of 2007 (e, f) and 2011 (g, h).

Table S1 List of precipitation total differences between perennial biofuel crop deployment experiments and Control experiments listed by according to experiment and deployment scenarios.

